

Journal of Materials Chemistry C

Accepted Manuscript



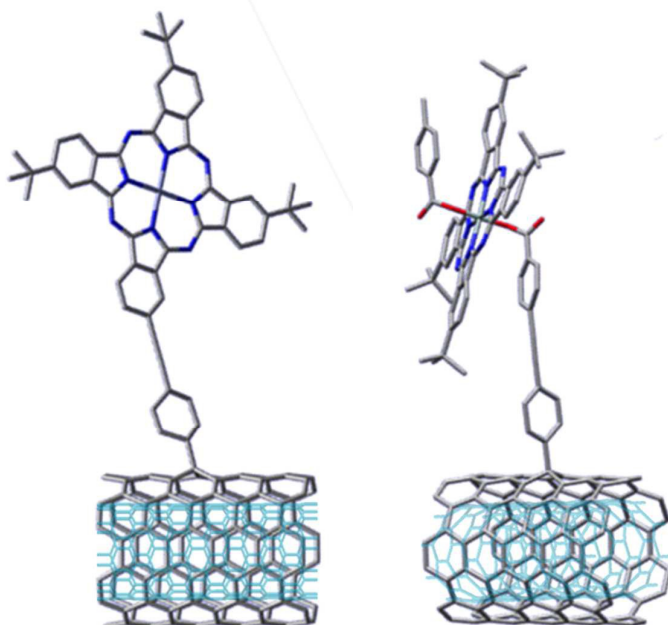
This is an *Accepted Manuscript*, which has been through the Royal Society of Chemistry peer review process and has been accepted for publication.

Accepted Manuscripts are published online shortly after acceptance, before technical editing, formatting and proof reading. Using this free service, authors can make their results available to the community, in citable form, before we publish the edited article. We will replace this *Accepted Manuscript* with the edited and formatted *Advance Article* as soon as it is available.

You can find more information about *Accepted Manuscripts* in the [Information for Authors](#).

Please note that technical editing may introduce minor changes to the text and/or graphics, which may alter content. The journal's standard [Terms & Conditions](#) and the [Ethical guidelines](#) still apply. In no event shall the Royal Society of Chemistry be held responsible for any errors or omissions in this *Accepted Manuscript* or any consequences arising from the use of any information it contains.

Table of Contents



Two new covalently bonded double wall carbon nanotube-phthalocyanine nano hybrids (DWCNT-ZnPc 1 and DWCNT-SiPc 2) hybrids with differently positioned phthalocyanine (connected through ring periphery or through axial bond) have been synthesized and characterized revealing different degree of ground and excited state interactions between both moieties. Absorbance, emission and electrochemical studies show electronic communication between the two active species. Femtosecond transient absorption and photocatalytic electron pooling studies were performed to seek evidence of charge separation in these hybrids.



Journal Name

ARTICLE

Peripheral *versus* Axial Substituted Phthalocyanine-Double-Walled Carbon Nanotube Hybrids as Light Harvesting Systems

Received 00th January 20xx,
Accepted 00th January 20xx

DOI: 10.1039/x0xx00000x

www.rsc.org/

Luis M. Arellano,^a Luis Martín-Gomis,^b Habtom B. Gobeze,^c Myriam Barrejón,^a Desiré Molina,^b María J. Gómez-Escalonilla,^a José Luis G. Fierro,^d Minfang Zhang,^e Masako Yudasaka,^e Sumio Iijima,^e Francis D'Souza,^{c,*} Fernando Langa^{a,*} and Ángela Sastre-Santos^{b,*}

Selective functionalization of the outer walls of double-walled carbon nanotubes (DWCNTs) with zinc and silicon phthalocyanines leaving the inner walls undamaged has been accomplished. The mode of metal phthalocyanine (MPc) connection was varied, that is, through macrocycle periphery in case of zinc phthalocyanine (ZnPc) and through silicon axial position in case of silicon phthalocyanine (SiPc) to visualize its effect on phthalocyanine-DWCNT interactions. Evidence of outer wall functionalization and degree of phthalocyanine substitution on DWCNT were arrived from HR-TEM, AFM, IR, TGA, XPS and Raman techniques. The sensitizer-nanotube interactions were probed from studies involving optical absorbance, and steady-state and time resolved emission, and electrochemical studies. The fluorescence of phthalocyanines in these hybrids was found to be almost quantitatively quenched (>95%) due to interactions with DWCNT, and such interactions were more for the SiPc derived hybrids. The performed femtosecond transient absorption studies revealed that the interactions are dynamic involving the singlet excited phthalocyanine and the nanotubes. In agreement with earlier studies, evidence for charge separation in these hybrids was weak revealing weak signature bands of MPc⁺ in the 850 nm range. Additionally, presence of trace amounts of single wall carbon nanotubes in the hybrids further hampered detailed spectral analysis.

Introduction

The use of carbon nanostructures, as principal components in donor-acceptor nanoensembles, is now experiencing a new impulse, primarily due to the actual momentum around graphene and graphene-based materials, but also because of current multigram availability of fine structure-controlled nanotube batches.¹ Carbon nanotubes (CNTs) have been always considered as a very promising class of carbon-based building blocks, suitable to construct hybrid materials with exceptional optoelectronic features, but the historic variability between batches has been, until now, a handicap that should be eluded in near future to afford its reliable employment in organic-based technological applications.² In spite of that, very interesting hybrid materials, based on the smart combination

of electron donor counterparts and CNTs, either by a classical covalent method³ or a non-covalent interaction, have been described.⁴ Nevertheless, neither of the strategies is perfect: while covalent bonding provides robust hybrid materials at the cost of sacrificing electronic properties, the supramolecular approach provides hybrids that are not very stable although this approach yields materials without introducing defects on the conjugated sp² carbon lattice.

DWCNT,⁵ due to the electronic communication between outer and inner walls,⁶ has recently emerged out as a convenient substitute for functionalized CNT hybrid materials as it combines all of the advantages found in the covalent and the supramolecularly functionalized hybrids. This strategy has been recently explored by us for the first time using perylene diimides (PDIs) as electron donor decorating agents, obtaining a series of DWCNT-PDI hybrids.^{7a} and more recently with antibodies.^{7b} However, although we were able to detect an effective electronic communication between inner and outer DWCNT walls where the inherent fluorescence of the PDI subunit was effectively quenched, the evidence of charge separation from the transient studies was weak, and accordingly, yields of photocatalytic electron pooling were much lower than those reported earlier for fullerene and single walled carbon nanotube based hybrids.

In this work we present DWCNTs covalently linked to good electron donor systems wherein we have been able to observe strong intramolecular interactions. We have chosen

^a Universidad de Castilla-La Mancha, Instituto de Nanociencia, Nanotecnología y Materiales Moleculares (INAMOL), 45071-Toledo, Spain. E-mail: Fernando.Langa@uclm.es

^b Área de Química Orgánica, Instituto de Bioingeniería, Universidad Miguel Hernández, Avda. de la Universidad, s/n, Elche 03202, Spain. E-mail: asastre@umh.es

^c Chemistry and Materials Science and Engineering, University of North Texas, 76203-5017 Denton, TX, USA. E-mail: Francis.DSouza@UNT.edu

^d Instituto de Catálisis y Petroleoquímica, CSIC, Cantoblanco, 28049, Madrid, Spain. E-mail: jlfierro@icp.csic.es

^e Nanotube Research Center, National Institute of Advanced Industrial Science and Technology, Higashi, Tsukuba, Ibaraki 305-8565, Japan

Electronic Supplementary Information (ESI) available: Synthesis and characterization of reference Pcs, experimental details, electrochemistry and nanosecond flash photolysis results. See DOI: 10.1039/x0xx00000x

phthalocyanines (Pcs),⁸ robust electron rich systems capable of forming long lived charge separated states,⁹ to synthesize two new DWCNT hybrids, DWCNT-ZnPc 1 and DWCNT-SiPc 2 (Chart 1). Moreover, we have studied the influence of the π -conjugate linker's effect on the DWCNT-Pc interactions using fully conjugated peripherally substituted zinc phthalocyanines and non-conjugated axially substituted silicon phthalocyanines. The structural properties of both DWCNT-phthalocyanine hybrids have been investigated via thermogravimetric analysis (TGA), X-ray photoelectron (XPS) and Raman spectroscopies, and transmission electron (TEM) and atomic force (AFM) microscopies. The photophysical properties of the DWCNT-Pc's derivatives have been studied by absorption and emission spectroscopic techniques in solution. This study is targeted to shed light on the electronic interactions between the electron donor phthalocyanine connected via conjugated and non-conjugated means to the outer wall of DWCNT, and its conducting inner tube. In these DWCNT-Pc hybrids, the inner tube would keep its (ideal) ballistic conducting behavior, being then capable to rapidly transport an electron to an external circuit, generated during the photoexcitation of the Pc, to be incorporated in the future in high efficient solar cells.

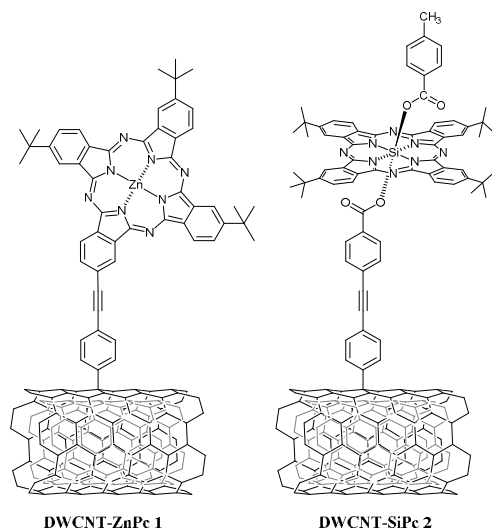
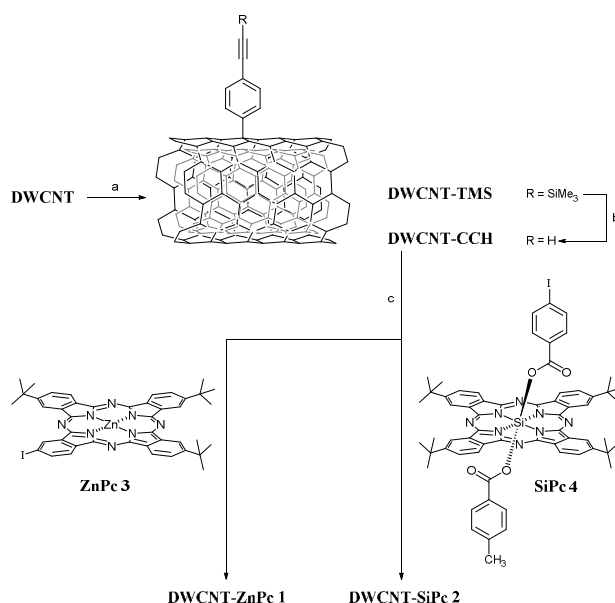


Chart 1: Structure of DWCNT-ZnPc 1 and DWCNT-SiPc 2.

Results and discussion

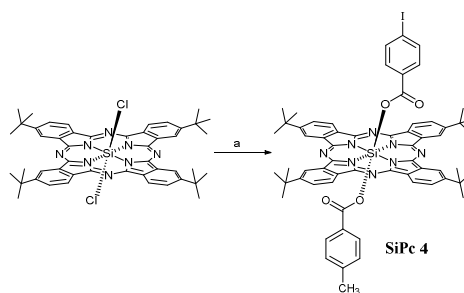
Synthesis and Characterization

The synthetic procedure for the preparation of the corresponding **DWCNT-ZnPc 1** and **DWCNT-SiPc 2** is illustrated in Scheme 1. Initially, *pristine* DWCNT was covalently functionalized by Tour reaction¹⁰ with 4-(2-trimethylsilyl)ethynylaniline in the presence of isoamyl nitrite affording **DWCNT-TMS**. Subsequent cleavage of the TMS groups using tetra-*N*-butylammonium fluoride (TBAF) gave **DWCNT-CCH**. Finally, **ZnPc 3** and **SiPc 4** were grafted onto the modified DWCNT using a Sonogashira C–C cross coupling reaction¹¹ affording the targeted nanohybrids **1** and **2**.

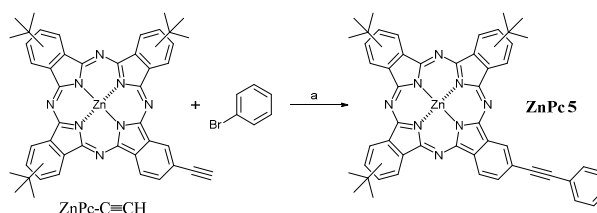


Scheme 1: Reagents and conditions: (a) 4-[(2-trimethylsilyl)ethynyl]aniline, isoamyl nitrite, NMP, 70 °C, 24 h; (b) TBAF, 0° C to rt, 3 h; (c) then, **Pc 3** or **Pc 4**, Pd₂(dba)₃, AsPh₃, NEt₃, DMF, 120°C, 4 days.

ZnPc 3 was obtained following a previously described procedure,¹² while asymmetric diaxially-substituted **SiPc 4** was synthesized, for the first time, from tetra-*tert*-butyl silicon dichlorophthalocyanine,¹³ and equimolar quantities of 4-iodobenzoic acid and 4-methylbenzoic acid (Scheme 2) using, in this case, microwave radiation to force double chloride substitution at the axial valences (see SI for experimental details).



Scheme 2: Reagents and conditions: (a) 4-iodobenzoic acid, 4-methylbenzoic acid, 1-butyl-3-methylimidazolium bromide, diglyme, microwave irradiation (200 MW, 200 °C, 15 min).



Scheme 3: Reagents and conditions: (a) Pd(PPh₃)₄, CuI, THF, Et₃N, Ar, 50 °C, 90 min.

Despite ZnPc is a good reference compound, we have also included Zn(II) tri(*tert*-butyl-4-(1'-phenyl)ethyl)phthalocyanine (**ZnPc 5**) as reference to get a more accurate study of the influence of the interactions of the ZnPc over the DWCNT and *vice versa*, ruling out the effect of the phenylethynyl bridge in the ground state electronic and redox properties of the hybrid **1**. **ZnPc 5** was synthesized (Scheme 3) following a modified synthetic route to the already published.¹⁴ Sonogashira coupling of (tri-*tert*-butylethynylphthalocyaninato)zinc(II)¹² with bromobenzene afforded **ZnPc 5** in 50 % yield (See SI).

DWCNT-Pc nanoconjugates **1** and **2** were characterized by Raman spectroscopy, thermogravimetric analysis (TGA), UV-vis absorption, X-ray photoelectron spectroscopy (XPS), transmission electron microscopy (TEM) and atomic force microscopy (AFM) as well as steady-state and time-resolved spectroscopic techniques to obtain fully detailed information about the structural, electronic and chemical properties of the functionalized double wall carbon nanotubes.

Thermogravimetric analysis (TGA) was applied to detect the degree of functionalization of the functionalized samples under inert atmosphere and at 600°C. The thermogram shown in Figure 1 revealed a weight loss about 4.1 % for *pristine* DWCNT, 16.6 % for DWCNT-TMS, 20.5 % for phthalocyanine hybrid DWCNT-ZnPc **1** and 51.2% for the control phthalocyanine **ZnPc 3**. The corrected weight losses due to the functional groups on nanotubes were then estimated to be 12.5 % for DWCNT-TMS and about 16.4 % for nanohybrid **1** (weight losses difference of DWCNT-TMS - *pristine* DWCNT and DWCNT-ZnPc **1** - *pristine* DWCNT). Accordingly, a degree of functionalization of one unit of organic fragments per about 110 carbon atoms for DWCNT-TMS could be estimated; with the same calculation, the amount of functional groups was 1 per 362 carbon atoms in nanohybrid **1**.

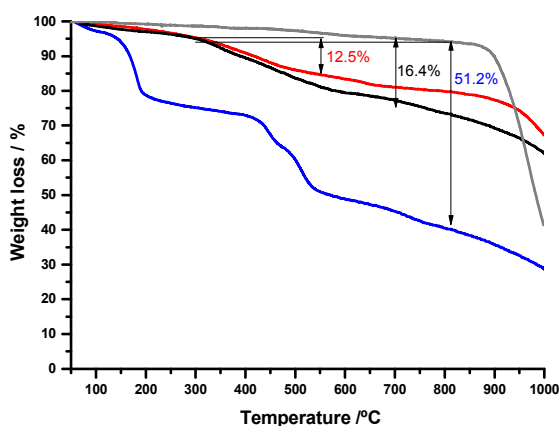


Figure 1: TGA curves of *pristine* DWCNT (grey), DWCNT-TMS (red), DWCNT-ZnPc **1** (black) and **ZnPc 3** (blue), (10 °C/ min under nitrogen).

In the case of nanohybrid **2**, the thermogravimetric analysis revealed a corrected weight loss of 14.2 %, 19.8 % and 51.5% (for DWCNT-TMS, DWCNT-SiPc **2** and SiPc **4** respectively). According with these results, the number of organic addends in DWCNT-TMS was estimated as 1 per 98 carbon atoms and

every 411 carbon atoms in DWCNT-SiPc **2** (Figure 2). The weight loss of 4.1 % at 600 °C observed for *pristine*-DWCNT may be due to the destruction of the residual amorphous carbon still present in the nanotubes and to the decarboxylation of the oxidized species.

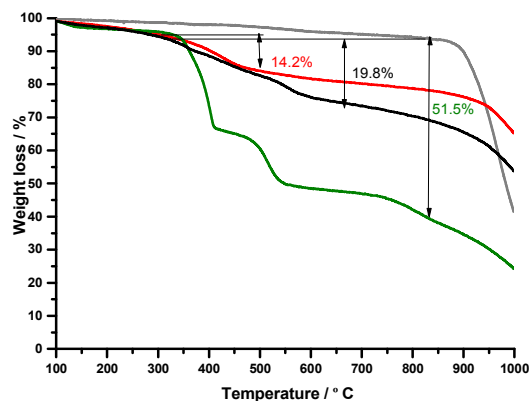


Figure 2: TGA profiles of *pristine* DWCNT (grey), DWCNT-TMS (red), DWCNT-SiPc **2** (black) and SiPc **4** (green), (10 °C/ min under nitrogen).

The functionalization procedure was also monitored by X-ray photoelectron spectroscopy (XPS). The binding energies of core levels of the elements and percentage of peak components of both DWCNT-Pcs and some of the raw reagents are summarized in Table S1 (see SI). Also included in this table are the BEs of core-levels of the elements of *pristine* DWCNT with that of Pcs (**ZnPc 3** and **SiPc 4**) and DWCNT-TMS intermediate employed in the synthesis of DWCNT-Pcs.

Fitting of the high resolution C1s spectrum of the *pristine* DWCNT sample (Figure S7 in SI) displayed the main component at 284.8 eV, due to sp² C on the DWCNT surface, and other minor components at 286.2, 287.7 and 289.2 eV assigned to C-O, C=O and COO groups respectively.¹⁵ Moreover, this C1s line shows a broad, weak component at about 291.3 eV, originated from the π-π* plasmon emission of C atoms in graphene-like structures.¹⁶ Similarly, the high resolution O 1s peak of DWCNT has been resolved with two components at 531.8 and 533.3 eV originated from O=C and O-C bonds present on the DWCNT surface.¹⁷

Table 1: XPS elemental composition of *pristine* DWCNT, *functionalized* DWCNTs samples and its precursors.

Sample	C (%at)	O (%at)	N (%at)	Si (%at)	Zn (%at)	I (%at)
ZnPc 3	84.6	-	12.5	-	1.4	1.5
SiPc 4	77.7	6.6	12.2	1.7	-	1.8
<i>pristine</i> DWCNT	95.1	4.9	-	-	-	-
DWCNT-TMS	96.3	3.1	-	0.6	-	-
DWCNT-ZnPc 1	93.3	3.0	3.3	-	0.4	-
DWCNT-SiPc 2	92.0	4.6	3.0	0.4	-	-

Upon anchoring the TMS group to DWCNT substrate, some changes in the C1s profile were observed: a minor contribution appeared at 285.3 eV, coming from the sp^3 C of the TMS group (see Figure S8), and simultaneously the $\pi-\pi^*$ plasmon emission disappeared. Quantitative data have also been obtained from XPS spectra. Surface composition of *pristine* DWCNT in terms of atom percentage is compiled in Table 1. The O-content of the *pristine* DWCNT is moderate (4.9%) and becomes reduced to 3.1% upon incorporation of TMS groups indicating that anchorage of TMS groups removes some of O-containing groups of the *pristine* DWCNT.

In addition, the BEs values of **DWCNT-Pcs 1** and **2**, and corresponding **ZnPc 3** and **SiPc 4** precursors are also summarized in Table S1. C 1s and O 1s emissions of **1** and **2** display contributions of both substrate and phthalocyanine precursors, together with N 1s and Zn 2p and Si 2p peaks originated from the phthalocyanine moieties. The N 1s peak of these functionalized samples was satisfactorily fitted to two components: the lower BE (398.7-398.8 eV) corresponding to six imine nitrogen atoms, while the peak at higher BE (400.3 eV) is associated to the two pyrrolic nitrogen atoms;¹⁸ the former peak is three times more intense than the latter. This observation is consistent with the molecular anchoring of the phthalocyanine moiety on the DWCNT substrate (see Table S1).

As shown in Table 1, indirect evidence for functionalization of the DWCNT with phthalocyanine groups comes from comparing atom percentages of C, O, N and Zn or Si in *functionalized* DWCNT samples. The similar Zn and Si percentage (0.4%) in both functionalized nanohybrids **1** and **2** indicates that the functionalization is almost the same degree in both materials, in agreement with TGA data.

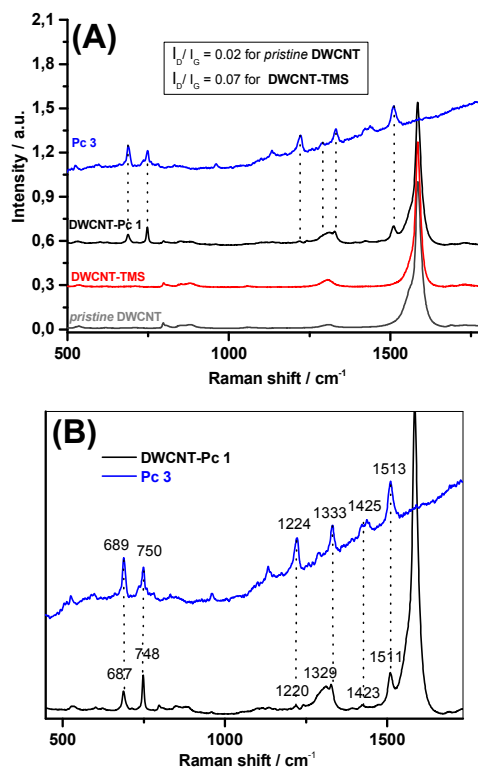


Figure 3: (A) Zoom of Raman spectra ($\lambda_{exc}=785$ nm) of *pristine* DWCNT (grey), **DWCNT-TMS** (red), **DWCNT-ZnPc 1** (black) and **ZnPc 3** (blue). Intensities have been normalized to the G-band (higher frequency); (B) the inset shows the presence of bands attributed to ZnPc moiety in **DWCNT-ZnPc 1**.

The sequence of the structural modification of DWCNT can be also followed by Raman spectroscopy (785 nm excitation) (Figure 3 and 4). *Pristine* DWCNT exhibit the two characteristic bands: the D mode (disordered-induced peak, sp^3 carbon) at around 1305 cm^{-1} and the G mode (1585 cm^{-1}) which correspond to the stretching mode in graphite (sp^2 carbons). As can be observed in Figure 3(A) and 4(A), the incorporation of the aryl moiety is traduced as an increase of the D band (which arises from the transformation of the sp^2 to sp^3 carbons), passing from $I_D/I_G = 0.02$ for *pristine* DWCNT to $I_D/I_G = 0.07$ for **DWCNT-TMS**. After second functionalization, the incorporation of **ZnPc 3** through the coupling reaction is reflected in the spectrum of **DWCNT-ZnPc 1**. In Figure 3(B) it is possible to find different peaks arising from **ZnPc 3**: at 1329, 1423 and 1511 cm^{-1} for the peaks relating to the vibrations of pyrrolic ring vibrations; the peak at 1420 cm^{-1} for the C-N stretching vibrations of the phthalocyanine structure as well as peaks at 687 and 748 cm^{-1} associated with the deformation of the macrocycle.¹⁹ These Raman spectra further prove that **DWCNT-Pc 1** has grafted with **ZnPc 3** moiety successfully.

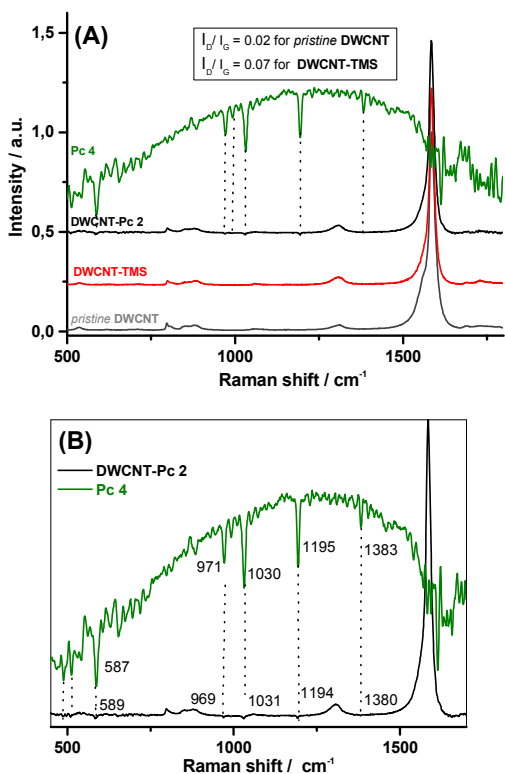


Figure 4: (A) Zoom of the Raman spectra ($\lambda_{exc}=785$ nm) of *pristine DWCNT* (grey), *DWCNT-TMS* (red), *DWCNT-SiPc 2* (black) and *SiPc 4* (green). Intensities have been normalized to the G-band (higher frequency); (B) the inset shows the presence of bands attributed to SiPc in *DWCNT-SiPc 2*.

Analogously, the bands related to **SiPc 4** are found in the Raman spectrum of the nanohybrid **2** (Figure 4): at 1383 and 1195 cm^{-1} (associated to the stretching vibrations of the pyrrole groups), and also the corresponding C-H in-plane vibrations of the benzene groups at 1030 cm^{-1} and 971 cm^{-1} .²⁰ This fact corroborates the covalent anchoring of **SiPc 4** onto the nanotube surface, in agreement with XPS data.

For both nanohybrids **1** and **2**, the G^+ -band appears at 1586 cm^{-1} , which is downshifted by 2 cm^{-1} as compared to that of starting DWCNT's peak at 1588 cm^{-1} (Figure 5). This result demonstrates that the electron-donor moiety linked onto the skeleton of double wall carbon nanotube is engaged in intramolecular interactions.²¹

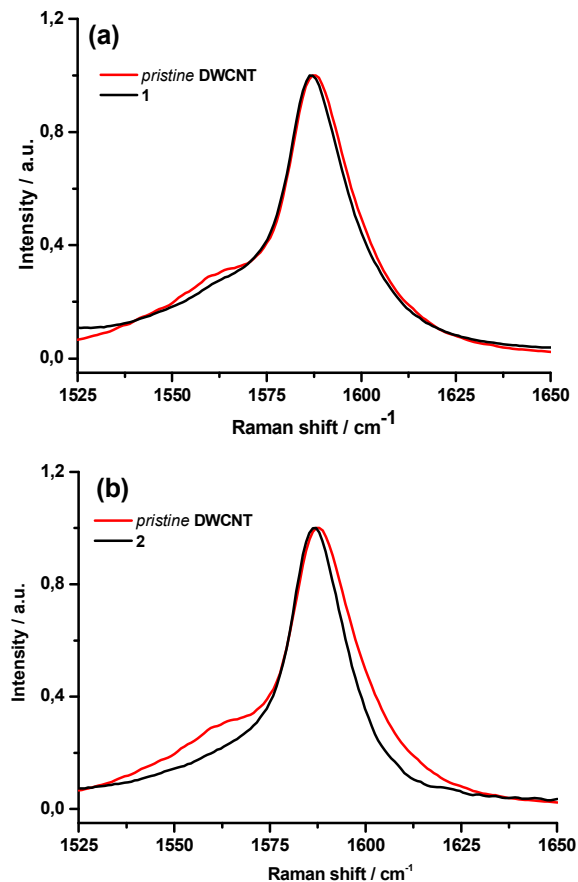


Figure 5: G-band region ($\lambda_{exc}=785$ nm) of (a) *pristine DWCNT* in comparison with nanohybrid **1** and (b) *pristine DWCNT* in comparison with nanohybrid **2**.

Regarding the radial breathing modes (RBM) (Figure 6), comparison of the spectra before and after Tour reaction shows that the RBM bands for the outer walls are reduced in their intensities, whereas the inner wall peaks are hardly affected. The retention of the inner tube suggests that the Tour reaction has a high selectivity on the outer walls of DWCNT.^{5a}

To further demonstrate the anchoring of the **Pcs** on the nanotube skeleton, we employed an atomic force microscope (AFM) to visualize the height increment of the materials. As shown in Figure 7, while starting DWCNT had an average height of ~ 2 nm (see Figure S9), after grafting the phthalocyanine moiety, the height increased to 3.9 nm (Figure 7a) for **ZnPc 3** and 4.2 nm in the case of **4** (Figure 7b); these height increments agree well with the lengths of phthalocyanine estimated from the more stable conformations obtained by means of molecular mechanics (~ 2 nm for both hybrids).

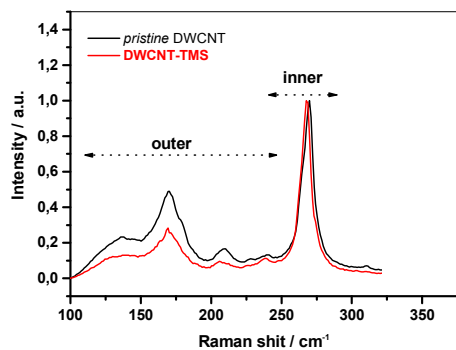


Figure 6: Comparative Raman spectrum from RBM zone (785 nm excitation) of *pristine* DWCNT (black), DWCNT-TMS (red). Arrows indicate the Raman shift regions where RBMs of the outer and inner tubes are observed.

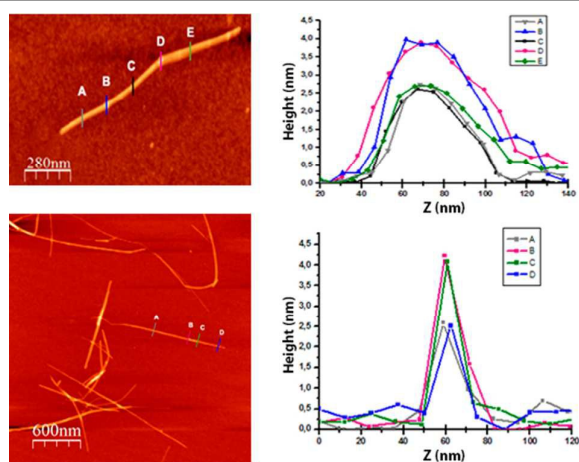


Figure 7: AFM topographic images of (a) DWCNT-ZnPc 1 and (b) DWCNT-SiPc 2 prepared by drop casting on a silicon wafer from a SDBS/water solution.

Concurring with the AFM results, the transmission electron microscopy (TEM) images revealed, materials of several nanometers in sizedecorated with Pcs in **1** and **2** (Figure 8)

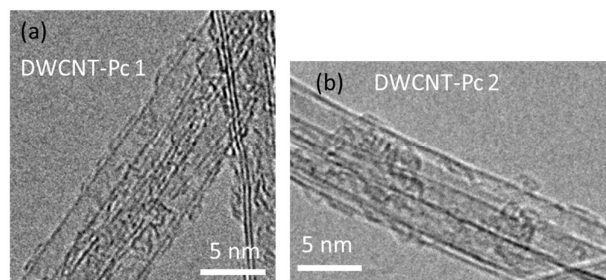


Figure 8: TEM images of (a) DWCNT-ZnPc 1 and (b) DWCNT-SiPc 2.

Electrochemical, spectroscopic and photophysical properties.

The electrochemical properties of **DWCNT-Pc 1** and **2** materials were studied by Osteryoung Square Wave Voltammetry (OSWV) and compared with the reference compounds **ZnPc 5** and **SiPc 4** respectively in benzonitrile

solution. In the nanohybrids, the first oxidation potentials are positively shifted by 60 mV in the case of **1**, and 20 mV for **2** respectively, relative to this corresponding phthalocyanine reference. Moreover, reduction of the DWCNT has changed and became a broad signal by the presence of the phthalocyanine and second oxidation and reduction processes of the phthalocyanine are influenced by the presence of the DWCNTs in the hybrids **1** and **2**. The Pcs second oxidation is not detected due to the interaction of the Pc with the DWCNT. In addition, the same interaction affects to the Pcs redox potential (See Fig S10 and S11). This suggests that the intramolecular interactions between the electroactive moieties are stronger in the fully conjugated **DWCNT-ZnPc 1** than in the non-conjugated **DWCNT-SiPc 2** hybrid.

Table 2: Electrochemical data determined by OSWV of carbon nanohybrids **1** and **2**, **ZnPc 5** and **SiPc 4**.^a

Compound	E_{ox1}/V	E_{ox2}/V	E_{red1}/V	E_{red2}/V
DWCNT-ZnPc 1	0.45		-1.46	
ZnPc 5	0.39	0.93	-1.52	-1.95
DWCNT-ZnPc 1	0.36 ^b	0.87 ^b	-1.44 ^b	
ZnPc 5	0.32 ^b		-1.48 ^b	
DWCNT-SiPc 2	0.56			-1.44
SiPc 4	0.54	1.04	-0.96	-1.48

^a Obtained in a benzonitrile solution containing 0.1 M TBAPF₆ and using Ag/AgNO₃ as a reference electrode, glassy carbon as working electrode and a Pt wire counter electrode. Scan rate is 100 mV/s. Potential are referenced to Fc/Fc⁺.^b Data obtained in a THF solution.

The presence of covalent bonded Pcs molecules in **DWCNT-Pc 1** and **2** was further supported by the spectroscopic study using UV-vis spectroscopy (recorded in DMF, PhCN and THF). The absorption spectra of the hybrid **DWCNT-ZnPc 1** and **ZnPc 5** and **DWCNT-SiPc 2** and **SiPc 3** are compared in Figure 9a and b respectively. The UV-vis spectrum of **ZnPc 5** registered in THF exhibits a typical metallophthalocyanine Q band split into two peaks at 691 and 681 nm, due to the inherent asymmetry of the molecule. These bands were slightly bathochromically shifted when the spectrum is recorded in PhCN. In the case of hybrid **1**, the Q-band is observed in both solvents together with a broad absorption from 700 to 800 nm indicating an effective conjugation, through a conjugated ethynylbenzyl linker, between the phthalocyanine and the DWCNT. This interaction is not observed when the Q-band absorption of **SiPc 4** 696 nm is compared with the Q-band in the hybrid **DWCNT-SiPc 2** centred and 698 nm.

Figure 10 a and b show steady-state fluorescence spectra of **DWCNT-ZnPc 1** and **DWCNT-SiPc 2** hybrids (uncorrected for DWCNT absorbance) along with their control compounds. **ZnPc 5** in DMF revealed an emission band at 679 nm along with a shoulder band at 742 nm. In the **DWCNT-ZnPc 1** hybrid, the 679 nm band was found to be blue-shifted by 2 nm with quenching of emission intensity as much as 95%. **SiPc 4** in

DMF revealed emission at 701 and 775 nm; interestingly, in the hybrid the intense peak was blue-shifted to 684 nm with quenching over 98%. These results reveal interactions between the phthalocyanine sensitizer and DWCNT. The 17 nm blue-shift of **SiPc 4** emission in the **DWCNT-SiPc 2** hybrid compared to the 2 nm blue-shift in **DWCNT-ZnPc 1** indicates that the **SiPc 4** functionalized via axial position interacts better than the **ZnPc 5** functionalized via ring periphery. The phthalocyanine fluorescence quenching in the hybrids could be due to either ground state complex formation (dark complex via inter- or intramolecular association) or dynamic quenching from the singlet excited phthalocyanine.

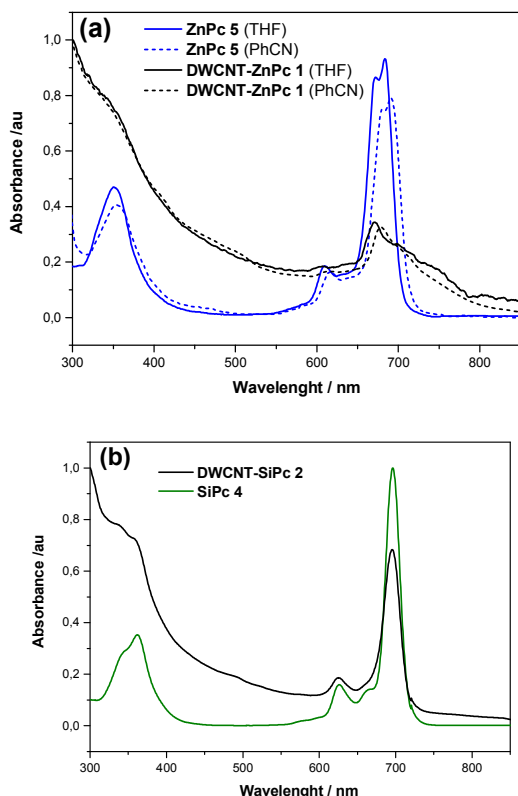


Figure 9: UV-vis spectra of (a) **ZnPc 5** and **DWCNT-ZnPc 1**, registered in THF and PhCN and (b) **SiPc 4** and **DWCNT-SiPc 2**, registered in PhCN.

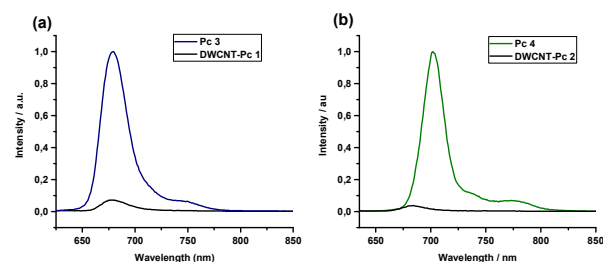


Figure 10: Steady-state fluorescence spectrum of (a) **ZnPc 5** and **DWCNT-ZnPc 1** hybrid ($\lambda_{\text{ex}} = 607$ nm) in DMF. (b) **SiPc 4** and **DWCNT-SiPc 2** hybrid ($\lambda_{\text{ex}} = 625$ nm) in DMF.

To clarify this, time resolved fluorescence using time correlated single photon counting (TCSPC) technique was performed. Both **ZnPc 5** and **SiPc 4** revealed monoexponential decay with lifetimes of 3.15 and 7.32 ns (see Figure S12 in SI), respectively. Our attempts to measure the lifetime of the phthalocyanine in the hybrids to differentiate these two mechanisms was not successful due to very low emission intensity and relatively high detection limit of lifetime setup (~ 200 ps). Further, femtosecond transient absorption studies have been performed to differential between the types of interactions and secure any evidence of charge separation in these hybrids.

First, femtosecond transient spectra of the probes, **ZnPc 5** and **SiPc 3** were recorded. As shown in Figure S13a, upon excitation of **ZnPc 5** (100 fs laser pulses of 400 nm), instantaneous singlet-singlet spectral features were observed with characteristic excited singlet peaks at 438, 478, 560, 630, 730, 840 and 1268 nm accompanied by transient bleaching at 607 and 676 nm, opposite of the absorbance spectral features of **ZnPc 5**.²² The 676 nm also had contributions from stimulated emission of **ZnPc**. The singlet features decayed/recovered slowly in accordance of **ZnPc** lifetime (3.15 ns) (see 13b for time profiles of 678 and 1300 nm peaks) with concomitant rise in the triplet features both in the visible and NIR region. The peak at 480 nm could be attributed to the $^3\text{ZnPc}^*$ state.²⁵ Similarly, **SiPc 4** immediately after excitation, revealed instantaneous formation of $^1\text{SiPc}^*$. Positive peaks at 603, 644, and 838 nm, and a negative peak at 694 nm were observed (Figure S13c). The negative peak corresponded to that of ground state bleaching and stimulated emission of **SiPc 4**. Scanning the spectrum into the near-IR region revealed broad spectral features with peak maxima at 1400 and 1476 nm corresponding singlet-singlet transition, similar to that observed for $^1\text{ZnPc}^*$. The time profile of the 694 nm corresponding to the ground state recovery and decay of the 1476 nm peak are shown in Figure 13d, respectively. These time profiles show slow recovery and decay of the signals in agreement with the relatively long fluorescence life time of **SiPc** (7.32 ns).

Excited state interactions in covalently and non-covalently linked phthalocyanine-single walled carbon nanotubes (Pc-SWCNT) are well known.^{23,24} Evidence for the occurrence of electron transfer has been secured from the transient and photocatalytic electron pooling experiments. Figure 11 shows the femtosecond transient spectra of **DWCNT-ZnPc 1** hybrids in DMF. At the excitation wavelength of 400 nm, instantaneous formation of singlet excited state of **ZnPc** was observed (spectrum at 0.49 ps). However, instead of slow intersystem crossing, the excited state decayed rapidly at a rate of about 10^{11} s^{-1} revealing efficient excited state interactions between the entities. New negative peaks at 566, 630, 701, 1080, 1206, and 1360 nm, at time constant less than 0.42 ps were observed. Recovery of the negative peaks was also rapid; in less than 3 ps most of the recovery process of was complete (recovery time constant = 1.22 ps). It is interesting to note that at 850 nm, weak spectral features attributable to ZnPc^+ were present (see Figure 11b).

Importantly, these results point out dynamic interactions as the main cause for the observed fluorescence quenching in Figure 10a.

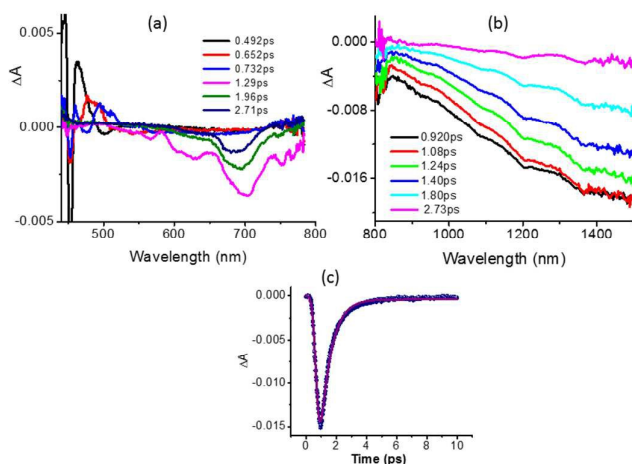


Figure 11. Femtosecond transient spectra of **DWCNT-ZnPc 1** in DMF at the indicated delay times (a) in the visible and (b) in the near-IR regions. The time profile of the 1200 nm peak is shown in panel c.

Similar results were also obtained in the case of **DWCNT-SiPc 2** hybrid. In this hybrid, initial SiPc singlet excitation was notable (spectrum at 0.32 ps in Figure 12a) which decayed rapidly at a rate of about 10^{11} s^{-1} revealing strong excited state interactions between SiPc and DWCNT. Subsequent relaxation of this peak revealed broad transient minima at 650 nm in the visible region and at 1200, 1370 and 1495 nm in the near-IR region with a time constant of about 0.42 ps (Figure 12c). Recovery of these peaks was rapid and occurred at a rate constant of 1.16 ps (see Figure 13c for the time profile). Weak spectral features around 840 nm could be observed in supportive of SiPc⁺, however, the strong transient minima hampered further analysis of this peak.

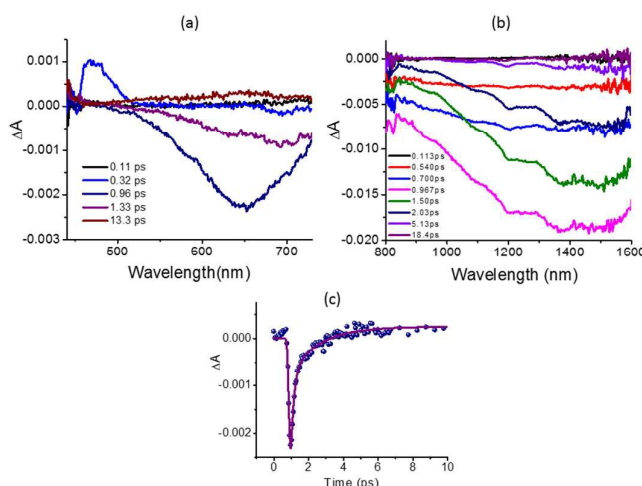


Figure 12. Femtosecond transient spectra of **DWCNT-SiPc 2** in DMF at the indicated delay times (a) in the visible and (b) in the near-IR regions. The time profile of the 650 nm peak is shown in panel c.

Nanosecond transient spectra of the hybrid was also recorded in DMF to seek evidence of charge separation from the ³MPC* (minor product of ¹MPC* intersystem crossing, M = Zn and Si). As shown in Figure S14 for **DWCNT-SiPc 1**, broad spectral features in the 800-870 nm range was observed. In the near-IR region covering 900-1250 nm range, few positive features were also observed, supporting rather weak charge separation process, if any.

The origin of the broad negative peaks in the visible and near-IR region in the case of both hybrids deserve special mention. It is known that sodium dodecylbenzene sulfonate (SDBS) micellar media exfoliates nanotubes effectively from which photoluminescence could be detected.²⁵ Tsyboulski et al. earlier reported photoluminescence studies of DWCNT in SDBS media and concluded that the observed weak emission is due to the trace amounts of SWCNT²⁶ present in the sample. The photoluminescence of **DWCNT-ZnPc 1** hybrid in SDBS was recorded as shown in Figure S15. Although much weak, peaks characteristic of SWCNT were observed suggesting presence of trace amounts of SWCNT²⁶ in the DWCNT used in the present study. This suggests that the SWCNTs could be responsible for the transient minima peaks seen in Figures 11 and 12. In fact, the spectral features and peak minima closely resemble that of Pc-SWCNT reported earlier.²⁴ These observations suggest weak charge separation in the **DWCNT-ZnPc 1** and **DWCNT-SiPc 2** hybrids although strong excited state interactions are noticed. It may be mentioned here that Aurisicchio et al.²⁷ made such a conclusion on porphyrin-DWCNT hybrids, which also corroborates our recent study on peryleneimide-DWCNT hybrids.⁷

Experimental

General

Ultra purity DWCNTs (catalog number: XNM-UP-11050, purified grade > 98%, length = 2 to 6 μm, diameter distribution 1-3 nm, average diameter: 2 nm) were purchased from XinNano Materials Inc (www.xinnanomaterials.com) and used without further purification treatment. All chemicals were reagent-grade, purchased from commercial sources, and used as received, unless otherwise specified. All air-sensitive reactions were carried out under Ar atmosphere. **ZnPc 3** was prepared following the experimental procedure described elsewhere.²⁸

DWCNT-TMS

DWCNT (50 mg) were first stirred in *N*-methyl-2-pyrrolidone (NMP) for 24 h, followed by sonication for 6 h and then 4-(2-(trimethylsilyl)ethynyl)aniline²⁹ (1.8 g, 8.3 mmol, 2 eq C) and isoamyl nitrite (1.3 mL, 10 mmol, 2.4 eq C) were. The reaction mixture was stirred at 70°C for 24 h under Ar. After cooling to room temperature, the crude was filtered over a PTFE (Millipore, 0.1 μm pore) membrane to separate the carbon-based material, which was subsequently sonicated in NMP and centrifugated. The supernatant was separated, and the solid residue resuspended in NMP, filtered again and was washed consecutively with methanol (MeOH) and dichloromethane

(CH₂Cl₂) until the filtrate was clear; finally was dried in vacuum oven at 40°C to afford a black solid (57.6 mg) as the product.

Deprotection of DWCNT-TMS

To a dispersion of DWCNT-TMS (10 mg, 0.83 mmol) in NMP (15 mL) was added a solution of tetra-*N*-butylammonium fluoride (TBAF, 1M in THF) (1.66 mmol). The reaction mixture was stirred under 0°C argon at room temperature for 3 hours, then filtered on PTFE (Millipore, 0.1 μm pore) membrane and washed consecutively with tetrahydrofurane, MeOH, acetone and CH₂Cl₂, to obtain the corresponding DWCNT-CCH such as a black solid and used directly for the next step.

General Procedure for the synthesis of DWCNT-Pcs hybrids

Pd₂(dba)₃ (2.09 mg, 2.29 μmol) and AsPh₃ (14.09 mg, 0.046 mmol) were dissolved in dry *N,N*-Dimethylformamide (DMF) (15mL) and subjected to several vacuum/argon cycles. Then, triethylamine (NEt₃) (0.5 mL) was added and subjected to more vacuum/argon cycles. Finally, DWCNT-CCH (10 mg) and the corresponding Pc (15 mg) were added to the reaction. The suspension was sonicated for 10 minutes and heater at 120°C for 4 days. After cooling to room temperature, the solid was separated by filtration through a PTFE (Millipore, 0.1 μm pore) membrane and washed extensively with DMF. Sonication and redispersion was repeated with acetone, MeOH and CH₂Cl₂ to remove the rest of the phthalocyanine and solvent; the colorless filtrate was checked by TLC (Thin Layer Chromatography) until the phthalocyanine had disappeared. Finally, the solid was dried overnight under vacuum oven at 40°C to afford the corresponding modified DWCNT-ZnPc **1** and DWCNT-SiPc **2** (17 mg and 14 mg, respectively).

Summary

In summary, the newly synthesized DWCNT-ZnPc **1** and DWCNT-SiPc **2** hybrids with differently positioned phthalocyanine (connected through ring periphery or through axial bond) reveal different degrees of ground and excited state interactions between the moieties. The synthetic protocols developed here allowed outer walls of the nanotube functionalization leaving the inner walls intact. With the help of HR-TEM, AFM, IR, TGA, XPS and Raman techniques, it was possible to rationalize the level of functionalization. Evidence for excited state interactions in these hybrids was secured from fluorescence (steady-state and time-resolved) and transient absorption spectral studies, with weak, if any, evidence for charge separation. The presence of trace amounts of SWCNT in the hybrids was witnessed from near-IR photoluminescence and transient absorption studies. Further studies to improve charge separation, photocatalytic activities and organic photovoltaic device characterization of DWCNT and SWCNT derived donor-acceptor hybrids are in progress in our laboratories.

Acknowledgements

This research was financially supported by the Spanish Ministry of Economy and Competitiveness (Mineco) of Spain (CTQ2011-26455, CTQ2013-48252-P and CTQ2014-55798-R), Generalitat Valenciana (Prometeo 2012/010), Junta de Comunidades de Castilla-La Mancha (PEII-2014-014-P) and the US-National Science Foundation (Grant No. 1401188 to FD).

Notes and references

- (a) D. Jariwala, V. K. Sangwan, L. J. Lauhon, T. J. Marks, and M. C. Hersam, *Chem. Soc. Rev.*, **2013**, *42*, 2824–2860; (b) K. Dirian, M. A. Herranz, G. Katsukis, J. Malig, L. Rodriguez-Perez, C. Romero-Nieto, V. Strauss, N. Martin, and D. M. Guldi, *Chem. Sci.*, **2013**, *4*, 4335–4353; (c) C. J. Shearer, A. Cherevan, and D. Eder, *Adv. Mater.*, **2014**, *26*, 2295–2318; (d) A. Stergiou, G. Pagona, and N. Tagmatarchis, *Beilstein J. Nanotechnol.*, **2014**, *5*, 1580–1589; (e) Bottari, G. de la Torre, and T. Torres, *Acc. Chem. Res.*, **2015**, *48*, 900–910.
- (a) W. Lu, M. Zu, J.-H. Byun, B.-S. Kim, and T.-W. Chou, *Adv. Mater.*, **2012**, *24*, 1805–1833; (b) M. F. L. De Volder, S. H. Tawfick, R. H. Baughman, and A. J. Hart, *Science*, **2013**, *339*, 535–539.
- (a) S. K. Das, A. S. D. Sandanayaka, N. K. Subbaiyan, M. E. Zandler, O. Ito, and F. D'Souza, *Chem. – A Eur. J.*, **2012**, *18*, 11388–11398; (b) R. Martín, F. J. Céspedes-Guirao, M. de Miguel, F. Fernández-Lázaro, H. García and Á. Sastre-Santos, *Chem. Sci.*, **2012**, *3*, 470–475; (c) M. E. Lipińska, S. L. H. Rebelo, M. F. R. Pereira, J. L. Figueiredo and C. Freire, *Mater. Chem. Phys.*, **2013**, *143*, 296–304; (d) P. d'Ambrosio, M. Carchesio, N. d'Alessandro, G. de la Torre, and T. T. Torres, *Dalt. Trans.*, **2014**, *43*, 7473–7479.
- (a) J. Bartelmeß, B. Ballesteros, G. de la Torre, D. Kiessling, S. Campidelli, M. Prato, T. Torres, and D. M. Guldi, *J. Am. Chem. Soc.*, **2010**, *132*, 16202–16211; (b) C. Backes, F. Hauke, and A. Hirsch, *Adv. Mater.*, **2011**, *23*, 2588–2601; (c) J. K. Sprafke, S. D. Stranks, J. H. Warner, R. J. Nicholas, and H. L. Anderson, *Angew. Chemie Int. Ed.*, **2011**, *50*, 2313–2316; (d) A. S. D. Sandanayaka, N. K. Subbaiyan, S. K. Das, R. Chitta, E. Maligaspe, T. Hasobe, O. Ito, and F. D'Souza, *ChemPhysChem*, **2011**, *12*, 2266–2273; (e) A. De Juan, Y. Pouillon, L. Ruiz-González, A. Torres-Pardo, S. Casado, N. Martín, Á. Rubio and E. M. Pérez, *Angew. Chemie - Int. Ed.*, **2014**, *53*, 5394–5400.
- (a) A. A. Green and M. C. Hersam, *ACS Nano*, **2011**, *5*, 1459–1467; (b) K. E. Moore, D. D. Tune and B. S. Flavel, *Adv. Mater.*, **2015**, *27*, 3105–3137.
- (a) M. Kalbac, A. A. Green, M. C. Hersam, and L. Kavan, *Chem. – A Eur. J.*, **2011**, *17*, 9806–9815; (b) M. Vizuete, M. J. Gómez-Escalonilla, S. García-Rodríguez, J. L. G. Fierro, P. Atienzar, H. García and F. Langa, *Chem. – A Eur. J.*, **2012**, *18*, 16922–16930.
- (a) M. Barrejon, S. Pla, I. Berlanga, M. J. Gómez-Escalonilla, L. Martín-Gomis, J. L. G. Fierro, M. Zhang, M. Yudasaka, S. Iijima, H. B. Gobeze, F. D'Souza, Á. Sastre-Santos, and F. Langa, *J. Mater. Chem. C*, **2015**, *3*, 4960–4969; (b) I. Ojeda, M. Barrejon, L. M. Arellano, A. González-Cortés, P. Yáñez-Sedeño, F. Langa and J.M. Pingarrón, *Biosensors and Bioelectronics*, **2015**, *74*, 24–29.
- (a) Phthalocyanines: Properties and Applications, ed. C. C. Leznoff and A. B. P. Lever, VCH, Weinheim, Germany, **1989**, vol. 1–4. (b) Phthalocyanines: Materials Synthesis Structure and Function, ed. N. B. McKeown, Cambridge University Press, Cambridge, **1998**.

- 9 (a) F. J. Céspedes-Guirao, L. Martín-Gomis, K. Ohkubo, S. Fukuzumi, F. Fernández-Lázaro and Á. Sastre-Santos, *Chem.–Eur. J.*, **2011**, *17*, 9153; (b) V. M. Blas-Ferrando, J. Ortiz, L. Bouissane, K. Ohkubo, S. Fukuzumi, F. Fernández-Lázaro and Á. Sastre-Santos, *Chem. Commun.*, **2012**, *48*, 6241; (b) V. M. Blas-Ferrando, J. Ortiz, K. Ohkubo, S. Fukuzumi, F. Fernández-Lázaro and Á. Sastre-Santos, *Chem. Sci.* **2014**, *5*, 4785.
- 10 J. Bahr and J. M. Tour, *Chem. Mater.*, **2001**, *13*, 3823–3824.
- 11 A. Aljarilla, J. N. Clifford, L. Pelleja, P. de la Cruz, F. Langa and E. Palomares, *J. Mater. Chem. A*, **2013**, *1*, 13640–13647.
- 12 E. M. Maya, P. Vázquez and T. Torres, *Chem.-A Eur. J.*, **1999**, *5*, 2004–2013.
- 13 D. C. Gale and J. G. Gaudiello, *J. Am. Chem. Soc.*, **1991**, *113*, 1610–1618.
- 14 H. Ali and J. E. Van Lier, *Tetrahedron Lett.*, **1997**, *38*, 1157–1160.
- 15 (a) H.P. Boehm, *Carbon*, **2002**, *40*, 145–149; (b) M. Vizuete, M. J. Gómez-Escalonilla, J. L. G. Fierro, P. Atienzar, H. García and F. Langa, *ChemPhysChem*, **2014**, *15*, 100–108.
- 16 A. Criado, M. Vizuete, M. J. Gómez-Escalonilla, S. García-Rodríguez, J. L. G. Fierro, A. Cobas, D. Peña, E. Guitian and F. Langa, *Carbon*, **2013**, *63*, 140–148.
- 17 A. Jung, R. Graupner, L. Ley and A. Hirsch, *Phys. Status Solidi*, **2006**, *243*, 3217–3220.
- 18 (a) K. H. Le Ho, L. Rivier, B. Jousselle, P. Jégou, A. Filoramo and S. Campidelli, *Chem. Commun.*, **2010**, *46*, 8731–8733; (b) R. L. Arechederra, K. Artyushkova, P. Atanassov and S. D. Minter, *ACS Appl. Mater. Interfaces*, **2010**, *2*, 3295–3302.
- 19 C. Jennings, R. Aroca, A. Hor and R. Loutfy, *J. Raman Spectrosc.*, **1984**, *15*, 34–37.
- 20 W. M. K. P. Wijekoon and S. P. Karna, *J. Raman Spectrosc.*, **1994**, *25*, 949–952.
- 21 (a) V. Straub, A. Gallego, G. de la Torre, T.W. Chamberlain, A. N. Khlobystov, T. Torres and D. M. Guldi, *Faraday Discuss.*, **2014**, *173*, 233–256; (b) R. Voggu, C. S. Rout, A. D. Franklin, T. S. Fisher and C. N. R. Rao, *J. Phys. Chem C*, **2008**, *34*, 13053–13056
- 22 (a) S. K. Das, A. Mahler, A. K. Wilson and F. D'Souza, *ChemPhysChem*, **2014**, *15*, 2462–2472. (b) C. B. KC, G. N. Lim and F. D'Souza, *Nanoscale*, **2015**, *7*, 6813–6826.
- 23 (a) F. D'Souza and O. Ito, *Chem. Commun.* **2009**, *33*, 4913; (b) A. S. D. Sandanayaka, N. K. Subbaiyan, S. K. Das, R. Chitta, E. Maligaspe, T. Hasobe, O. Ito and F. D'Souza, *ChemPhysChem* **2011**, *12*, 2266–2273; (c) S. K. Das, N. K. Subbaiyan, F. D'Souza, A. S. D. Sandanayaka, T. Wakahara and O. Ito, *J. Porphyrins Phthalocyanines*, **2011**, *15*, 1033–1043; (d) R. Chitta, A. S. D Sandanayaka, A. L. Schumacher, L. D'Souza, Y. Araki, O. Ito and F. D'Souza, *J. Phys. Chem. C*, **2007**, *111*, 6947–6955; (e) F. D'Souza, A. S. D. Sandanayaka and O. Ito, *J. Phys. Chem. Lett.* **2010**, *1*, 2586–2593; (f) F. D'Souza, S. K. Das, M. E. Zandler, A. S. D. Sandanayaka and O. Ito, *J. Am. Chem. Soc.*, **2011**, *133*, 19922 – 19930.
- 24 (a) J. Bartelmess, A. R. Soares, M. Martínez-Díaz, N. Victoria, G. P. M. S. Miria, A. C. Tome, J. S. Cavaleiro, T. Torres and D. M. Guldi, *Chem. Commun.*, **2011**, *47*, 3490–3492; (b) J. Bartelmess, B. Ballesteros, G. de la Torre, D. Kiessling, S. Campidelli, M. Prato, T. Torres and D. M. Guldi, *J. Am. Chem. Soc.*, **2010**, *132*, 16202–16211; (c) U. Hahn, S. Engmann, C. Oelsner, C. Ehli, D. M. Guldi and T. Torres, *J. Am. Chem. Soc.* **2010**, *132*, 6392–6401; (d) G. Bottari, G. de la Torre, D. M. Guldi and T. Torres, *Chem. Rev.* **2010**, *110*, 6768–6816; (e) B. Ballesteros, S. Campidelloi, G. de la Torre, C. Ehli, D. M. Guldi, M. Prato and T. Torres, *Chem. Commun.* **2007**, *28*, 2950–2952; (f) B. Ballesteros, G. de la Torre, C. Ehli, G. M. A. Rahman, R. Agullo-Ruedo, D. M. Guldi and T. Torres, *J. Am. Chem. Soc.* **2007**, *129*, 5061–5068; (g) D. M. Guldi, A. Gouloumis, P. Vazquez, T. Torres, V. Georgakilas and M. Prato, *J. Am. Chem. Soc.* **2005**, *127*, 5811–5813.
- 25 J. G. Duque, L. Cognet, A. Nicholas, G. Parra-Vasquez, N. Nicholas, H. K. Schmidt and M. Pasquali, *J. Am. Chem. Soc.* **2008**, *130*, 2626–2633.
- 26 D. A. Tsybouski, J.-D. R. Rocha, S. M. Bachilo, L. Cognet and R. B. Weisman, *Nano Lett.*, **2007**, *7*, 3080–3085.
- 27 C. Aurisicchio, R. Marega, V. Corvaglia, J. Mohanraj, R. Delamare, D. A. Vlad, C. Kusko, C. A. Dutu, A. Minoia, G. Deshayes, O. Coulembier, S. Melinte, P. Dubois, R. Lazzaroni, N. Armaroli and D. Bonifazi, *Adv. Funct. Mater.*, **2012**, *22*, 3209–3222.
- 28 E. M. Maya, P. Vazquez and T. Torres, *Chem. Commun.*, **1997**, 1175.
- 29 J.-J. Hwang and J. M. Tour, *Tetrahedron*, **2002**, *58*, 10387–10405.